Published OnlineFirst October 16, 2018; DOI: 10.1158/2326-6066.CIR-18-0179

Research Article

Cancer Immunology Research

Phage-Based Anti-HER2 Vaccination Can Circumvent Immune Tolerance against Breast Cancer

Caterina Bartolacci[1], Cristina Andreani[1], Claudia Curcio[2,3], Sergio Occhipinti[3], Luca Massaccesi[4], Mirella Giovarelli[3], Roberta Galeazzi[4], Manuela Iezzi[2], Martina Tilio[1], Valentina Gambini[1], Junbiao Wang[1], Cristina Marchini[1], and Augusto Amici[1]

Abstract

Δ16HER2 is a splice variant of HER2 and defined as the transforming isoform in HER2-positive breast cancer. It has been shown that Δ16HER2 promotes breast cancer aggressiveness and drug resistance. In the present work, we used *in silico* modeling to identify structural differences between Δ16HER2 and the wild-type HER2 proteins. We then developed DNA vaccines specifically against the Δ16HER2 isoform and showed that these immunotherapies hampered carcinogenesis in a breast cancer transplantable model. However, the vaccines failed to elicit immune protection in Δ16HER2 transgenic mice because of tolerogenic mechanisms toward the human HER2 self-antigen, a scenario commonly seen in HER2$^+$ patients. Thus, we engineered bacteriophages with immunogenic epitopes of Δ16HER2 exposed on their coat for use as anticancer vaccines. These phage-based vaccines were able to break immune tolerance, triggering a protective anti-Δ16HER2 humoral response. These findings provide a rationale for the use of phage-based anti-HER2/Δ16HER2 vaccination as a safe and efficacious immunotherapy against HER2-positive breast cancers. *Cancer Immunol Res; 6(12); 1486–98.* ©*2018 AACR.*

Introduction

The high incidence of breast cancer makes the development of new therapies an urgent need. The tyrosine kinase (TK) receptor HER2 is overexpressed in roughly 20% to 30% of breast cancer patients and correlates with poor prognosis (1–3). HER2 is an ideal target for cancer immunotherapies. The introduction into the clinic of the HER2 monoclonal antibody (mAb) trastuzumab improved the overall survival and time-to-disease progression of patients with HER2-positive ($^+$) breast cancer (4). However, many patients do not benefit from treatment because of therapy resistance (5). Active immunotherapy against HER2 might, thus, represent an alternative strategy (6). Unfortunately, despite the promising results obtained in preclinical models, anti-HER2 vaccination has shown only modest clinical effects, and to date, there are no breast cancer vaccines approved by the FDA (7). Breaking immune tolerance represents a major obstacle in tumor vaccine technology. HER2 is a self-antigen, and effective immunization needs to overcome the patient's self-tolerance. A naturally occurring HER2 splice variant lacking exon-16 (Δ16HER2) has emerged as the HER2 oncoprotein variant responsible for transformation (8–12). The deletion removes cysteine residues within the HER2 extracellular domain (ECD), disrupting the disulfide bond structure of the protein and fostering the formation of stable constitutively activated homodimers, which fuel downstream mitogenic signaling (13, 14). Δ16HER2 is expressed in 52% to 90% of human HER2$^+$ breast cancers (9–11, 15). Of the patients expressing Δ16HER2, 90% suffer from metastatic disease. Increasing evidence points to a role for the Δ16HER2 splice variant in resistance to trastuzumab (10) and lapatinib (16). Thus, a successful strategy against HER2$^+$ breast cancer implies the suppression of Δ16HER2. However, no specific Δ16HER2 therapies are available yet.

Here, we unraveled structural differences between Δ16HER2 and the wild-type (wt)HER2 proteins. We then generated DNA and phage-displayed vaccines against wtHER2 and Δ16HER2 to optimize antigen presentation, break tolerance against HER2 self-protein, and induce selective immune responses discriminating between the two isoforms. The proposed antigen-delivery system derives from the Large Fragment Phage-Display (LFPD) technology (17). Briefly, benign filamentous bacteriophage M13 virions are engineered to display the extracellular and transmembrane (TM) domains of human wtHER2 or Δ16HER2 (hECTM and Δ16ECTM, respectively) or specific HER2 epitopes on their surface as fusion proteins with the coat protein pIII. In particular, we

[1]Department of Biosciences and Veterinary Medicine University of Camerino, Camerino, Italy. [2]Aging Research Centre, G. d'Annunzio University, Chieti, Italy. [3]Department of Molecular Biotechnology and Health Sciences, Center for Experimental Research and Medical Studies, University of Torino, Torino, Italy. [4]Dipartimento di Scienze della Vita e dell'Ambiente, Università Politecnica delle Marche, Ancona, Italy.

Note: Supplementary data for this article are available at Cancer Immunology Research Online (http://cancerimmunolres.aacrjournals.org/).

C. Bartolacci and C. Andreani contributed equally to this article.

Corresponding Authors: Augusto Amici, University of Camerino, via Gentile III Da Varano, Camerino 62032, Italy. Phone: 39-0737-403275; Fax: 39-0737-636216; E-mail: augusto.amici@unicam.it; and Caterina Bartolacci, Phone: 39-0737-403275; E-mail: caterinabartolacci@gmail.com

doi: 10.1158/2326-6066.CIR-18-0179

Published OnlineFirst October 16, 2018; DOI: 10.1158/2326-6066.CIR-18-0179

focused on epitopes 6–11, which overlap the splicing region (between exons 15 and 17) and the adjacent trastuzumab binding site. The anticancer activity of these vaccines was assessed in Δ16HER2 mice (18), which are suitable for testing anti-HER2 therapies (16, 19) because they develop spontaneous aggressive mammary carcinomas and exhibit immunologic tolerance to human HER2 antigen, mimicking what is encountered clinically.

Materials and Methods

In silico modeling

To identify the complete structure of wtHER2, we adopted the strategy of "building in blocks," taking advantage of PDB data bank structural information. In particular, PDB 3BE1 (20) and PDB 3N85 (21) files entirely contained the ECD, with two loops (aa 101–110 and aa 362–366) and the juxtamembrane region left out. The TM domain was completed in PDB 2JWA (22, 23). Because the TK domain has not been fully crystallized, the structure was truncated at residue Glu1028, the last available amino acid (PDB 3PP0; ref. 24). We obtained the juxtamembrane region via homology modeling using the highly homologous HER1 crystal structure (identity score of 75, 83%) as a template (PDB 3GOP; refs. 25, 26). 3D modeling was performed using Sculptor software implemented in the Schrödinger Suite 10. Moodloop (27), GalaxyWEB (28), and SWISS-MODEL (29) were used to model loops. DISULFINID (30) web server was used to score the probability of disulfide bonds to occur (score range 0–10, with higher values indicating higher probability). CHARMM-GUI membrane builder (31) was used to simulate the lipid bilayer. The simulation box was set to $155 \times 155 \times 243$ Å^3.

Preparation for the productive MD simulation on the wtHER2, Δ16HER2 with the disulfide bond between Cys626 and Cys630 (Δ16HER2-SS) and Δ16HER2 with reduced Cys626 and Cys630 (Δ16HER2-free), was carried out with a seven-step minimization and equilibration protocol with CHARMM 36 force field. Cycles (10,000) of steepest descent energy minimization, followed by a 5,000 step of conjugate gradient minimization, were sufficient for the maximum force to converge to the energy threshold of 1,000 (kJ/mol/nm). The following six equilibration steps were conceived to let the protein gradually accommodate within the lipidic and aqueous environment. In all runs, the Verlet cutoff scheme was used for neighbor searching, combined with PME for electrostatics. The cutoff for the calculation of Van der walls forces was set to 1.2 nm, with the force smoothly switched to zero between 1.0 and 1.2 nm. Velocities were first generated at 310 K in the NVT ensemble, using a Maxwell distribution function with random seed, and a weak temperature coupling (Berendsen thermostat) with time constant of 1 ps was applied to maintain the reference temperature (310 K) for the whole run. Protein, membrane, and solvent were coupled in distinct groups. After two short simulation runs of 25 ps each, we shifted to the NTP ensemble maintaining the weak coupling also for pressure control (i.e., Berendsen barostat). For the third 25 ps long simulation run, semi-isotropic conditions were set, with a reference pressure of 1 bar and a time constant for coupling of 5 ps. For the three remaining equilibration runs, only the number of steps was changed, from 25 ps to 50 ps. Position restraints were applied to both protein and membrane. From step 1 to step 5, the protein and the membrane were slowly accommodated by gradually reducing the restraints force constants. We started with 1,000 kJ/mol nm^2 for lipid solvent and a stronger 4,000 kJ/mol nm^2 for protein, until we completely freed all particles at the beginning of the sixth equilibration step. The described protocol was applied to all three systems (wtHER2, Δ16HER2-SS, and Δ16HER2-free). At the beginning of the production phase, we shifted to Nosé-Hoover for temperature control and Parrinello-Rahman algorithm for pressure coupling. Ten-nanosecond-long dynamic simulation was run for each system, implementing an accurate leapfrog algorithm or integrating Newton's equations of motion, with a time step of 0.002 ps.

Mice

Δ16HER2 transgenic mice (18) and FVB mice (FVB/NCrl strain from Charles River) were housed under controlled temperature (20°C) and circadian cycle (12 hours light/12 hours dark) in the animal facility of University of Camerino. The animals were fed on chow diet (Mucedola) and tap water *ad libitum*. Female FVB mice were used in all experiments to match tumor prone Δ16HER2 female mice according to genetic background and sex. All animal experiments were carried out in accordance with the U.K. Animals (Scientific Procedures) Act, 1986 and associated guidelines, EU Directive 2010/63/EU for animal experiments. All the procedures were approved by the Ethic Committee on Animal Use of the University of Camerino (protocol number 14/2012).

Cell lines

Cam6 (16), N202.1A, and N202.1E cells (kindly provided by Prof. Pier Luigi Lollini, University of Bologna, Italy) were cultured in Dulbecco Modified Eagle Medium (DMEM) supplemented with 20% fetal bovine serum (FBS; Thermo Fisher Scientific) and 1% penicillin/streptomycin (P/S). HEK293-nontransfected cells were maintained in 10% FBS and 1% P/S DMEM. HEK293 Δ16HER2 and HEK293 wtHER2, a generous gift from the Unit Department of Experimental Oncology-Istituto Nazionale Tumori di Milano, were maintained in G418 antibiotic (Gold Biotechnology, 1 mg/mL). SKBR3 (ATCC) were maintained in McCoy's 5a Modified Medium (ATCC) enriched with 10% FBS. All the cell lines were maintained at 37°C in an atmosphere of 5% CO_2.

DNA vaccines

pVAX-hECTM and pVAX-HuRT were generated as previously described (32, 33). pVAXΔ16ECTM was obtained by PCR and inserted in pVAX1 (Invitrogen), using standard cloning methods. *Escherichia coli* strain DH5a was transformed with the different plasmids and then grown in Luria-Bertani medium with kanamycin (Sigma-Aldrich). The sequences of the obtained plasmids were verified by sequencing (BMR Genomics). Large-scale preparation of the plasmids was carried out by alkaline lysis using Endofree Qiagen Plasmid-Giga kit (Qiagen Inc.) according to the manufacturer's instructions. Subsequently, DNA was resuspended in sterile bidistilled water and stored in aliquots at −20°C, after concentration determination using NanoDrop spectrofotometer (Thermo Scientific).

DNA vaccination

The vaccination consisted of two intramuscular (i.m.) injections (into the tibial muscle) of 50 μg of the plasmids described above, followed by electroporation using T820 electroporator (BTX), 2 square-ware 25 ms, 375 V/cm pulse. In wtFVB mice, immunization with the different DNA vaccines was carried out

Published OnlineFirst October 16, 2018; DOI: 10.1158/2326-6066.CIR-18-0179

21 and 7 days before retro-orbital bleeding (8 mice per group) to collect sera. One day after sera collection, mice were challenged with 10^5 Cam6 cells inoculated into the mammary fat pad. In Δ16HER2-transgenic mice, DNA vaccination was performed with two boosts at 8 and 10 weeks of age. Two weeks after the last boost, blood was collected from the orbital sinus under anesthesia. All of the animals were monitored weekly by palpation to assess tumor onset. Tumor diameter was measured by digital caliper. Masses greater than 2 mm in mean diameter were regarded as tumors.

Analysis of antibody response

In order to collect serum, whole blood samples were left to clot at room temperature for 20 minutes. Serum separation was accomplished by two subsequent centrifugations at 2000 × *g* at 4°C. Sera, collected 7 days after the second vaccination, from immunized mice were analyzed by flow cytometry (BD FACSCalibur), using HEK293 Δ16HER2 cells, and nontransfected HEK293 cells as negative controls.

Briefly, subconfluent HEK293 Δ16HER2 or HEK293 cells were detached and dispensed at a density of 10^6 cells per tube. After a 5-minute centrifugation at 800 rpm at 4°C, the obtained cell pellet was resuspended and washed twice in staining buffer (2% FBS-containing 1× PBS, pH 7.4). Cells were incubated with sera of vaccinated mice (1:40 dilution in staining buffer) for 1 hour at 4°C. MGR2 antibody (kindly provided by E. Tagliabue, Department of Experimental Oncology-Istituto Nazionale Tumori, Milano) was used as positive control (10 μg/mL in staining buffer). After incubation, cells were washed three times and incubated with the goat anti-mouse IgG (H+L) secondary antibody-FITC (Thermo Fisher Scientific, 1:200 dilution in staining buffer). Samples were washed twice, resuspended in 600 μL of staining buffer and analyzed using BD FACSCalibur. Cell Quest Pro (version 6.0.2) and FlowJo (version 8.7) were used as acquisition and analysis software, respectively.

To verify the presence of antibodies against the rat-HER2/*neu* and the human-HER2 proteins in the sera of Δ16HER2 transgenic mice, collected 14 days after the last immunization, we used N202.1A cells and SKBR3 cells, respectively. Ab4 (Oncogene Research Products/EMD Biosciences) and Ab5 (Calbiochem/EMD Millipore) monoclonal antibodies were used as positive controls.

Analysis of IgG isotypes

Sera collected from Δ16HER2 transgenic mice 14 days after the second pVAX-HuRT immunization were pooled together and diluted 1:40 in staining buffer, as described in the above section. Antibody isotype was evaluated by FACS analysis (BD FACS Calibur). Briefly, N202.1A cells or SKBR3 cells were incubated with diluted sera for 1 hour at 4°C, washed, and stained with biotin-conjugated rat anti-mouse antibodies specific for IgA, IgM, IgG1, IgG2a, IgG2b, and IgG3 (Invitrogen Caltag Laboratories). Cells were further washed and incubated with streptavidin–phycoerythrin (PRE; Dako; 1:20 dilution) for the next 30 minutes.

Purification of IgG evoked by vaccination on FVB mice

IgGs were purified from sera of wtFVB vaccinated mice using the Melon Gel IgG Purification Kit (Thermo Fisher Scientific) and quantified using NanoDrop spectrophotometer using IgG settings (Thermo Scientific). Sample purity was in the range of $A_{260}/A_{280} < 0.6$.

Cellular ELISA assay

HEK293, HEK293 Δ16HER2, and HEK293 wtHER2 cells were collected (5 minutes, 800 rpm centrifugation) and dispensed in 96-well polystyrene round-bottom microplates (Orange Scientific) at a cell density of 2×10^5 cells/well. After a blocking step with 10% BSA-PBS, purified IgGs were added at different concentrations 30, 60, or 100 μg/mL. The plates were left to incubate for 1 hour at 37°C and washed prior to a 1-hour incubation with the anti-mouse peroxidase-conjugated secondary antibody (Calbiochem, 1/3,000 dilution). Bound antibodies were detected adding 2,2′-azino-bis (3-ethylbenzothiazoline-6-sulfonic acid) substrate (Sigma), and the reaction was read at 405 nm. Wells, where only the secondary antibody was added, were used to measure the background noise. Each condition was repeated in triplicate.

Phages production and purification

All the HER2 and Δ16HER2 fragments (Δ16ECTM, ECTM, Ep6-11Δ16ECTM, and Ep6- 11ECTM) were cloned in frame with gIIIp of M13K07 Helper Phage (NEB) to generate phage-displayed clones, using the phage-display technique.

For this purpose, we adapted the previously described LFPD library (17) that is able to express large peptide sequences (100 amino acid-long) as fusions to the coat proteins of bacteriophages. Briefly, to produce the recombinant M13 phages, TG1 cells containing phagemids were grown in 2xYT medium with 100 μg/mL ampicillin and glucose 1% w/v at 37°C. When optical density at 600 nm reached OD = 0.4, bacterial cells were infected by the phage KO7M13 (NEB) at a multiplicity of infection (moi) of 20, incubated for 30 minutes at 37°C without shaking and 30 minutes at 37°C with shaking. Bacterial cultures were then centrifuged for 15 minutes at 3,600 rpm. The pellets were resuspended in 2xYT medium with 100 μg/mL ampicillin, 25 μg/mL kanamycin, and IPTG 200 μmol/L and incubated overnight at 30°C. Phages released overnight in the supernatant were purified by with 3:10 v/v ratio of PEG-NaCl. Phages were pelleted by centrifugation for 2 hours at 4,000 rpm and 4°C, and then resuspended in 2 mL of PBS. All eluates (approximately 2 mL/L of bacteria) were pooled and further centrifuged at 13,000 rpm for 2 minutes to pellet the remaining impurities. Phages were filtered through a 0.22-μm Millipore filter and titrated by top-agar plaque assay. The concentration of virion particles was further verified by spectrometry, according to the following formula: $\text{virions/mL} = [(A_{269} - A_{320})/ \times 6 \times 10^{16}]/(\text{number of bases/virion})$.

Affinity phage ELISA assay

An ELISA assay was carried out using phages expressing whole hECTM and Δ16ECTM molecules or just epitopes 6 and 11 and pooled sera derived from immunized wtFVB mice. 10^{11} phages/well were let to adsorb to 96-well microtiter plates (Maxisorb, NUNC) at 4°C, overnight. The day after, wells were blocked with 10% BSA-PBS, and increasing concentrations of IgGs purified from the pooled sera (from 0.5 to 100 μg/mL) were added. After 1 hour of incubation and 5 washings (PBS/Tween 20), peroxidase-conjugated goat anti-mouse secondary antibody (Calbiochem, 1:3,000) was added. Empty phages were used as negative controls, and phage-coated wells incubated with only the secondary antibody were included to identify background noise. Bound IgGs were detected with 2,2′-azino-bis (3-ethylbenzothiazoline-6-sulfonic acid) substrate (Sigma). Absorbance was read at 405 nm. Each experimental condition was tested in quadruplicate.

Published OnlineFirst October 16, 2018; DOI: 10.1158/2326-6066.CIR-18-0179

Avidity phage ELISA assay

The phage ELISA protocol was modified as follows: after incubation with IgGs (20, 60, or 100 μg/mL), half of the wells were rinsed with PBS, while urea at increasing concentrations (from 0.1 to 8 mol/L, in PBS) was added in the others. Plates were incubated for 10 minutes at 37°C and washed 5 times before adding the goat anti-mouse secondary antibody (Calbiochem, 1:3,000). Phage-coated wells with just urea or PBS were used to normalize the data. Each experimental condition was tested in quadruplicate using the same parameters as above.

Competitive phage ELISA assay

Microplates were coated with 10^{11} phages/well (either hECTM phages or Δ16ECTM phages). IgGs (60 μg/mL) were mixed with increasing amounts of competitor phage (10^6 to 5×10^{11} per well): Δ16ECTM phages for hECTM phage-covered wells, and vice versa. Each experimental condition was tested in quadruplicate. A set of four wells, where the competitor phage with no primary antibody was added, was used to exclude false-positive results.

Bone marrow dendritic cell generation and transfection

Cells (1×10^6) derived from bone marrow of both FVB and Δ16HER2 mice were cultured in complete medium (10% FBS, 2 mmol/L L-glutamine, 1% P/S RPMI1640 100 supplemented with 20 μg/mL mouse granulocyte–macrophage colony-stimulating factor, mGM-CSF). Expression of CD11c was evaluated by flow cytometry (CD11c-PerCP/Cy5.5, clone N418, BioLegend; 1 μg/mL). DCs were harvested using Pan Dendritic Cell Isolation Kit mouse (MACS, Miltenyi Biotec) according to the manufacturer's instructions, resuspended in 100 μL of electroporation buffer (mouse Dendritic Cell transfection kit, Amaxa, Lonza), and mixed with 5 μg of plasmid DNA. After electroporation, cells were cultured at 37°C for 2 days before undergoing further applications.

T-cell activation and flow-cytometric analysis for granzyme B and IFNγ on activated splenocytes

DCs electroporated with pVAX-hECTM, pVAX-Δ16ECTM, or pVAX-HuRT were cultured with splenocytes recovered from Δ16HER2 transgenic mice immunized with the corresponding plasmid at 1:10 ratio in RPMI1640 medium with 10% FBS. Three days after, IL2 (10 UI/mL) was added to the culture. Seven days later, splenocytes were recovered, and 1×10^6 cells were restimulated with coated anti-CD3 (10 μg/mL; clone 17A2, BioLegend) in the presence of Brefeldin A (10 μg/mL; Sigma-Aldrich). After 18 hours, splenocytes were stained with anti-CD8 FITC (clone 53-6.7, BioLegend, 2 μg/mL) and anti-CD4 PerCP/Cy5.5 (clone GK1.5, BioLegend, 2 μg/mL). Following incubation with Brefeldin A (5 μg/mL; Sigma-Aldrich) intracellular cytokine staining for IFNγ and granzyme B was performed using a BD Fixation/Permeabilization kit (BD Biosciences) according to the manufacturer's instructions. Anti-IFNγ–PE (clone XMG1.2, BioLegend; 2 μg/mL) and anti-granzyme B–AlexaFluor 647 (clone GB11, BioLegend, 5 μg/mL) were used. Data were acquired by FACS analysis (BD FACS Calibur) and IFNγ- and granzyme B-positive cells were expressed as percentage of CD8$^+$ T cells using FlowJo software (version 8.7).

CD107 mobilization assay

DCs were transfected with pVAX-hECTM, pVAX-Δ16ECTM, or pVAX-HuRT. After 2 hours, splenocytes recovered from Δ16HER2 transgenic mice immunized with the corresponding plasmid were added to the transfected DCs with the splenocyte/DC ratio being 5:1. Anti-CD107 (clone 1D4B, BioLegend, 1 μg/mL) was simultaneously added, and mixed cells were allowed to incubate for 1 hour. After that, monensin (5 μg/mL) was added to prevent acidification of endocytic vesicles for additional 4 hours. After 5 hours of DC/splenocyte coculture, splenocytes were collected and stained with antibodies for specific regulatory T cell (Treg) markers: FITC-conjugated anti-CD4 (BioLegend, at 2 μg/mL), PerCP/Cy5.5-conjugated anti-CD25 (clone 3C7, BioLegend, at 2 μg/mL), and anti-Foxp3 PE (clone 150D/E4, eBioscience). In the latter case, samples were first fixed and permeabilized as described. The same experiments were carried out using wtFVB mice as negative controls.

Adoptive transfer of immune sera

Immune sera from previously immunized wtFVB mice, equal to 60 μg/mL IgG, were infused by intraperitoneal (i.p.) route in Δ16HER2 females, from the 10th week of age. The treatment was performed weekly until the mice were sacrificed (at 20 weeks of age).

Phage immunization

Δ16HER2 mice were inoculated intraperitoneally with 0.1 mL of phage preparation (1×10^{10} PFU/mouse) at 8 and 10 weeks of age. Four experimental groups (8 mice/group) were designed, receiving Δ16ECTM phages, hECTM phages, Ep6-11 Δ16ECTM phages, or Ep6-11 hECTM phages. Control mice were injected with 0.1 mL of empty phages. Blood was collected from the retro-orbital plexus before and 2 weeks after the second boost to verify antigen-specific antibodies. Throughout the experiment course, mice were weekly monitored for tumor onset by palpation. Masses were measured by means of a digital caliper (masses greater than 2 mm in diameter were regarded as tumors).

CD3$^+$ and CD8$^+$T tumor-infiltrating cells upon phage vaccination

Tumors removed from phage-vaccinated mice were fixed in 4% PFA and frozen in a cryo-embedding medium (OCT, BioOptica). Sections (5 μm thick) were stained with hematoxylin and eosin and immunostained with either anti-CD8α (BD Pharmingen) or rabbit polyclonal anti-mouse CD3 (ab828, Abcam). After incubation with the appropriate secondary antibody, immunostaining was developed with Vulcan Fast Red (Biocare) alkaline phosphatase method in the case of CD8 staining, whereas EnVision rabbit and DAB (DAKO, K4065) were used for CD3 staining. Intratumoral CD8- or CD3-positive cell count was performed in 10 microscopic fields (×200 magnification) per tumor.

Antibody-dependent cell-mediated cytotoxicity (ADCC) on sera of Δ16HER2 mice vaccinated with either phages or DNA plasmids

Cam6 cells were used as target cells. Briefly, Cam6 (10^6/mL) were stained with carboxyfluorescein succinimidyl ester (CFSE, 5 μmol/L final concentration) at 37°C for 10 minutes in the dark. The next day, freshly isolated splenocytes (effector:target ratio of 1:2.25) and immune sera (1:200 dilution) were added to target cells and left to incubate at 37°C overnight. The following day, effector cells were washed out and target cells were incubated with propidium iodide (0.5 μg/mL), harvested, and analyzed by

Published OnlineFirst October 16, 2018; DOI: 10.1158/2326-6066.CIR-18-0179

flow-cytometric analysis. Cells incubated with splenocytes (no serum) were used to normalize the results.

Phage circulation in mice

Mouse serum was separated from blood by double centrifugation at 2,250 × *g*. Titers of viable phages were determined as described above by top-agar plaque assay plating serial serum dilutions (50 μL) on bacterial cultures distributed on the surface of dried agar plates. The plates were incubated overnight at 37°C. All experiments were repeated three times.

mRNA extraction from the thymus of Δ16HER2 transgenic mice and PCR analysis

Total RNA was extracted and purified from thymuses of wtFVB and Δ16HER2 mice at 3 weeks of age using TRIzol reagent (Invitrogen Life Technologies). cDNA was synthesized with the High-Capacity cDNA Reverse Transcription Kit of Applied Biosystems SuperScript following the manufacturer's instructions. PCR was performed using the following Δ16HER2 specific pair of primers (10): Forward 5′-CACCCACTCCCCTCTGAC-3′; Reverse 5′-GCTCCACCAGCTCCGTTTCCTG-3′. Primers that amplify GAPDH (BD Clontech) were used as standard.

mRNA extraction from mammary adenocarcinoma and PCR analysis

Tumor masses in Δ16HER2 mice were surgically excised, and their dimensions were evaluated by means of a caliper. In particular, the excised mammary adenocarcinomas were 2 × 2 mm, 3.6 × 3.1 mm, and 6.2 × 5.4 mm in diameter. Total RNA was extracted, and cDNA was synthesized as described above. PCR was performed using the following pair of primers to specifically detect murine ecto-5′-nucleotidase CD73 (NM_011851): Forward 5′-CAAATCCCACACAACCACTG-3′; Reverse 5′-TGCTCACTTGGTCACAGGAC-3′. Primers that amplify GAPDH (BD Clontech) were used as standard.

Statistical analysis

Quantitative data are presented as means ± SD from three independent experiments. The significance of differences was evaluated with an unpaired Student *t* test when two groups were compared, while one-way ANOVA test followed by the Tukey posttest was used to compare three or more groups. Two-way ANOVA test followed by the Tukey posttest was used to compare three or more groups over time. For Kaplan–Meier curves, a log-rank (Mantel–Cox) test was used. Statistical analysis was carried out with GraphPad Prism5. Detailed statistical analysis for each experiment is reported in the correspondent Supplementary Tables (S1-S25).

Results

Loss of exon 16 enhances flexibility and mobility of Δ16HER2 isoform

Leveraging *in silico* modeling, we first completed the wtHER2 structure (Fig. 1A). We then moved to Δ16HER2, and we considered the possibility that the cysteine residues left unpaired upon the deletion form novel disulfide bonds. The DISULFINID webserver (31) provided low output scores, 2 and 3 over 10, for Cys623-Cys600 and Cys626-Cys630, respectively. Although Cys623–Cys600 interaction was excluded, we did not completely rule out the occurrence of a Cys626–Cys630 bond

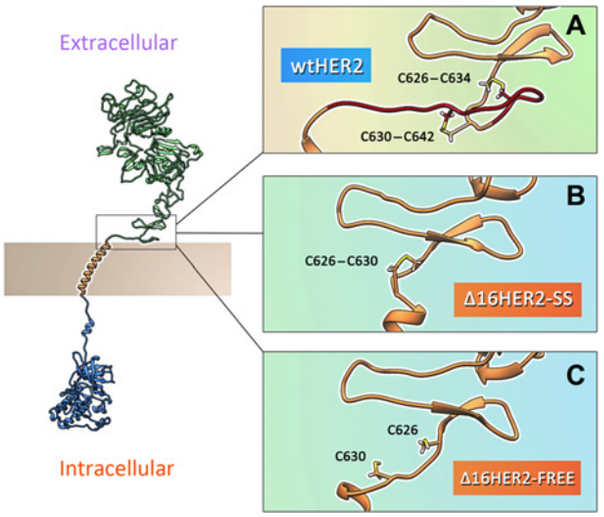

Figure 1.

In silico prediction of Δ16HER2 and wtHER2 interactions with the cell membrane. The figure shows the front view of the three models of HER2 taken into consideration. **A,** The wild-type form (wtHER2). **B,** The Δ16HER2 splice variant with the disulfide bond between Cys626 and Cys630 (Δ16HER2-SS). **C,** Δ16HER2 with reduced Cys626 and Cys630 (Δ16HER2-free). The juxtamembrane domain is firmly secured within the membrane in wtHER2, considerably limiting its mobility, while in both Δ16HER2-SS and Δ16HER2-free it sets free from stabilizing interactions with the membrane components.

(score 3 = mild confidence). Accordingly, we obtained three models: the wtHER2, Δ16HER2 with the disulfide bond between Cys626 and Cys630 (Δ16HER2-SS), and Δ16HER2 with reduced Cys626 and Cys630 (Δ16HER2-free; Fig. 1A–C, respectively).

The three models were oriented using the OMP server and inserted into the virtual membrane; we looked at the dynamic behavior of the 641-CPAEQRASP-650 sequence, which connected the ECD to the TM domain (Fig. 1). In wtHER2, polar (Gln629, Gln646, Thr631, and Ser649) and basic (Arg647 and His632) residues placed this stretch within the phospholipid heads. Principal component analysis suggested that this sequence secured the ECD within the membrane, limiting its mobility with just a bending of the I/II/III subdomains toward the IV subdomain. Consequently, the dimerization arm in this subdomain constantly faced the TM domain, immobilized in the initial alignment throughout the 10 ns of run. Arguably, the stability of the ECD was compromised upon the deletion of exon16 in both Δ16HER2-SS and Δ16HER2-free—the dimerization arm lost its alignment to end over the N-terminus, with the shortened connecting sequence completely extending into the solvent medium, free of the stabilizing interactions with membrane components. Hence, the ECD, aside from the minor twisting observed for the canonical protein, gained a considerable degree of rotation of almost 60° (Supplementary Video S1 *in silico* simulation comparing wtHER2 vs. ΔHER2).

Protective immunity elicited by anti-Δ16HER2 DNA vaccination in wtFVB mice

We first verified the protective efficacy of pVAX-hECTM and pVAX-Δ16ECTM DNA vaccines in a transplantable tumor

Published OnlineFirst October 16, 2018; DOI: 10.1158/2326-6066.CIR-18-0179

model using Δ16HER2-expressing Cam6 cells (16). pVAX-hECTM encodes the EC and TM domains of wtHER2, whereas pVAX-Δ16ECTM encodes the EC and TM domains of Δ16HER2 (Fig. 2A). The empty pVAX vector and pVAX-HuRT were used as negative and positive controls, respectively. pVAX-HuRT encodes for a human–rat chimeric protein composed by the first and second human (Hu) EC subdomains of HER2 protein and by the third and fourth rat (R) EC subdomains plus rat TM region. The syngeneic portion of the sequence ensures the specificity of the immune response, and the xenogeneic part ensures a better suppression of tolerance (refs. 32, 33; Fig. 2A). The regimen comprised two boosts, performed 21 and 7 days before bleeding (Fig. 2B). Kaplan–Meier curves showed that all the tested vaccines (pVAX-Δ16ECTM, pVAX-hECTM, and pVAX-HuRT) completely inhibited tumor development up to 100 days after tumor challenge, leading to 100% tumor-free survival, whereas all the control mice vaccinated with pVAX empty vector developed tumors within 25 days, as expected (Fig. 2C; ****, $P < 0.0001$; for detailed statistical analysis, refer to Supplementary Table S1). Extending the follow-up to 200 days after tumor challenge, pVAX-Δ16ECTM emerged as the most effective vaccine. Almost 60% of the immunized mice remained protected until the end of the experiment (Fig. 2C). Consistently, serum screening for Δ16HER2 antibodies on HEK293 cells stably transfected with Δ16HER2 (HEK293 Δ16HER2) revealed that all three DNA vaccines (pVAX-hECTM, pVAX-Δ16ECTM, and pVAX-HuRT) were able to induce an antibody response that significantly correlated with the observed anticancer protection. In particular, despite the intragroup variability, sera from mice vaccinated with pVAX-Δ16ECTM had higher antibody titers than the cohort of mice vaccinated with pVAX-hECTM (Fig. 2D; ****, $P < 0.0001$; for detailed statistical analysis, refer to Supplementary Table S2).

pVAX-Δ16ECTM and pVAX-hECTM evoked antibodies with different properties

To explain the differential efficacy displayed by pVAX-Δ16ECTM and pVAX- hECTM, we took into consideration the antibody–antigen interaction. Specifically, we focused on immunoglobulin G (IgG) because it contributes to antibody-based immunity. We set up a cellular ELISA incubating HEK293 cells stably transfected with either Δ16HER2 (HEK293 Δ16HER2) or wtHER2 (HEK293 wtHER2) with IgGs purified from sera of mice vaccinated with pVAX (IgG pVAX), pVAX-hECTM (IgG hECTM), or pVAX- Δ16ECTM (IgG Δ16ECTM). In this *in vitro* system, IgG Δ16ECTM and IgG hECTM showed differing results. On HEK293 wtHER2 cells, the binding of IgG hECTM significantly outweighed IgG Δ16ECTM (Supplementary Fig. S1A, central panel; ****, $P < 0.0001$). Binding curves of IgG hECTM and IgG Δ16ECTM almost overlapped with each other on HEK293 Δ16HER2 cells with no significant differences (Supplementary Fig. S1A, right; Supplementary Table S3). We hypothesized that the higher flexibility of Δ16HER2, in comparison with wtHER2, interfered with the stability of the antibody binding, so that it was difficult to identify specific Δ16HER2 antibodies using this analytical system. Consistent with our hypothesis, the kinetics of the antibody–antigen interaction showed that the binding occurred very rapidly in HEK293 wtHER2, especially for IgG hECTM. According to the modeling data herein described, we concluded that the rigid distribution of the wtHER2 antigen in the plane of the membrane promoted the binding of specific antibodies. Thus, IgG hECTM binds to wtHER2 antigen more rapidly than IgG

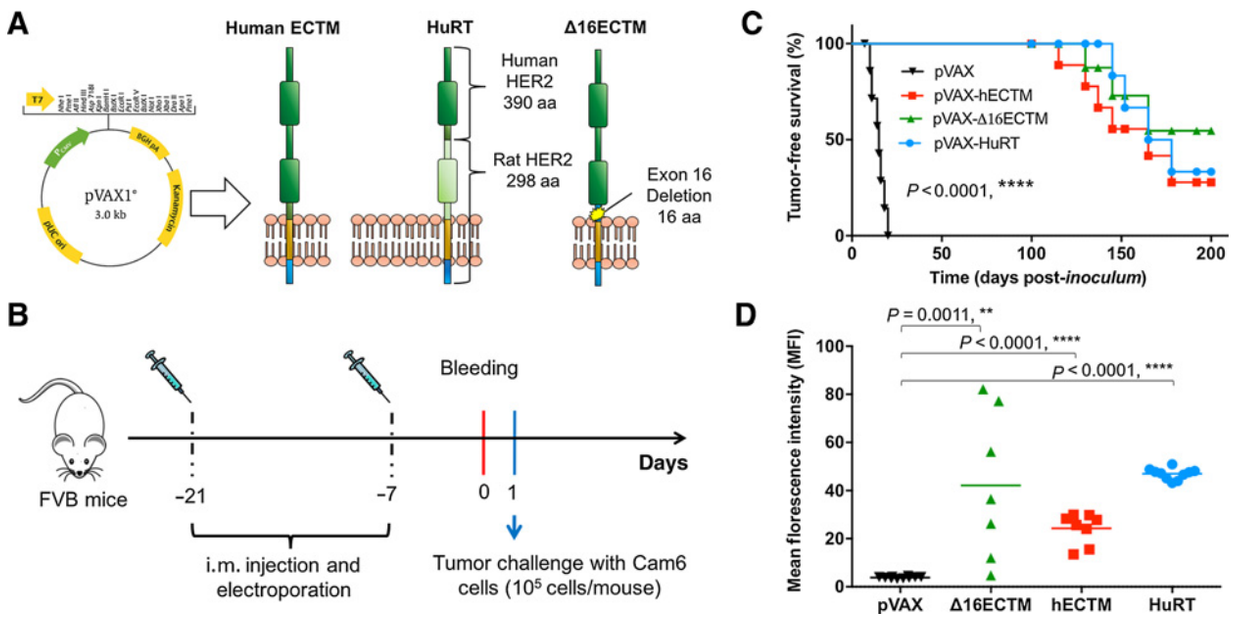

Figure 2.

Immunogenicity of anti-HER2 and anti-Δ16HER2 vaccines in wtFVB mice transplanted with Δ16HER2$^+$ mammary tumor cells. **A,** Tested vaccines: pVAX-hECTM, pVAX-Δ16ECTM, pVAX-HuRT, and pVAX empty vector. **B,** Vaccination regimen. Mice ($n = 8$ mice/group) underwent two DNA vaccine boosts at 7 and 21 days before the tumor cells challenge. **C,** Kaplan–Meier curves of pVAX-Δ16ECTM, pVAX-hECTM, and pVAX-HuRT vaccinated mice (log-rank test, ****, $P < 0.0001$; see Supplementary Table S1). **D,** Screening of sera from vaccinated mice for the presence of anti-Δ16HER2 by flow-cytometric analysis (see Supplementary Table S2).

Published OnlineFirst October 16, 2018; DOI: 10.1158/2326-6066.CIR-18-0179

Δ16ECTM, saturating the absorbance signal in 10 minutes of incubation (Supplementary Fig. S1B, left; ****, $P < 0.0001$; Supplementary Fig. S1C). For detailed statistical analysis, refer to Supplementary Tables S4 and S5. However, when we turned to HEK293 Δ16HER2, the binding of both IgG hECTM and IgG Δ16ECTM peaked lower values, even after 60 minutes (Supplementary Fig. S1B, right). It was possible that the high flexibility permitted cross-reactivity (both IgG hECTM and IgG Δ16ECTM equally bind to HEK293 Δ16HER2) but at the expense of low-affinity binding interactions because of the unfavorable entropy changes (34). Because antigen–antibody binding is mediated by noncovalent interactions (35), the change in the conformational freedom might pose a selective pressure on the repertoire of bound IgGs.

We suggest that only the high-affinity antibodies are selected for clonal expansion *in vivo*. This data interpretation would reconcile with the enhanced protection offered by pVAX-Δ16ECTM vaccine. Thus, we used the LFPD library, a cell-free IgG screening method, to better analyze the properties of IgG binding excluding the effects due to the plasma membrane itself. As previously described (17), we used the M13K07 Helper Phage and the pIF6 phagemid vector to generate phages carrying sequences in-frame encoding both their pIII protein and the amino acid sequence of interest (Supplementary Fig. S2A). We generated phages exposing the whole EC and TM domains of wtHER2 or Δ16HER2 (hECTM phages and Δ16ECTM phages, respectively) and phages harboring the epitopes 6–11 (Ep6–11 hECTM phages and Ep6–11 Δ16ECTM phages) because these epitopes cover the splice junction of Δ16HER2 (between exons 15 and 17; Supplementary Fig. S2B; ref. 17). Once quantified using traditional plaque assay and UV absorbance spectra (Supplementary Fig. S2C), phage particles were used as immobilized antigens to analyze affinity, avidity, and specificity of the antibody–antigen interaction. We evaluated the affinity as the increase in the fraction of antigen-bound antibodies over a range of antibody concentrations (Fig. 3A–E; Supplementary Table S6). On the empty phages, no signal was recorded (Fig. 3A). The absorbance values (Abs_{405}) measured for IgG hECTM outweighed those related to IgG Δ16ECTM in wells where hECTM phages were previously adsorbed (Fig. 3B, at 60, 80, and 100 μg/mL; ****, $P < 0.0001$), and the result was reversed for Δ16ECTM phages (Fig. 3C). Ep6-11 phages mirrored the trends seen for their respective whole-molecule counterparts, although with lower absorbance values. On Ep6-11 hECTM phages, the saturation binding curve for IgG hECTM had a significantly sharper slope and peaked higher than the IgG Δ16ECTM (at 2 μg/mL; $P = 0.002$, Fig. 3D), with the opposite scenario on Ep6-11 Δ16ECTM phages (Fig. 3E). To evaluate the avidity, the phage ELISA was modified adding increasing concentrations of urea after antibody binding. The dissociation curves point to a tighter binding of distinct IgG to their specific antigen. Greater concentrations of urea were

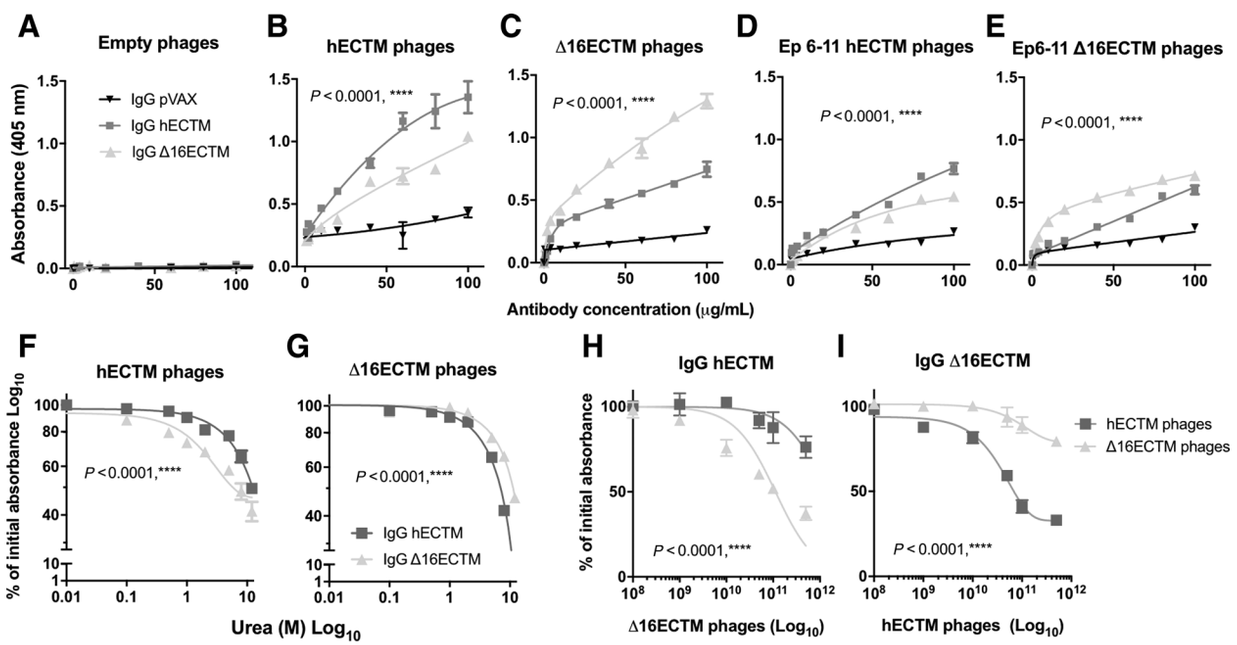

Figure 3.

Antigen-binding properties of IgGs elicited in wtFVB mice by DNA vaccination. **A–E,** IgG pVAX, IgG hECTM, and IgG Δ16ECTM from sera of vaccinated FVB mice were added to wells coated with phages ($n = 8$ mice/group pooled and assayed in quadruplicates). **A,** IgGs binding curve to empty phages. **B–E,** IgG hECTM and IgG Δ16ECTM binding curves to hECTM phages, Δ16ECTM phages, Ep6–11 hECTM phages, and Ep6–11 Δ16ECTM phages (see Supplementary Table S6). **F** and **G,** Avidity ELISA assay. **F,** IgG hECTM and IgG Δ16ECTM dissociation curves from hECTM phages in the presence of urea. **G,** IgG hECTM and IgG Δ16ECTM dissociation curves from Δ16ECTM phages in the presence of urea. Data are reported as percentage of the initial absorbance (i.e., without urea; see Supplementary Table S7). **H** and **I,** Competitive ELISA assay. IgGs were mixed with increasing amounts of the competitor phages. **H,** Binding curves for IgG hECTM to hECTM phages in the presence of increasing Δ16ECTM phages. **I,** Binding curve of IgG Δ16ECTM to Δ16ECTM phages in the presence of increasing hECTM phages. Experiments were performed in quadruplicate. Data are reported as percentage of the initial absorbance (i.e., without the competitor phages) (see Supplementary Table S8 for statistics). Data of each panel are representative of three independent experiments.

Published OnlineFirst October 16, 2018; DOI: 10.1158/2326-6066.CIR-18-0179

required to dissociate IgG hECTM from hECTM phages and IgG Δ16ECTM from Δ16ECTM phages (Fig. 3F and G; Supplementary Table S7). To address the antibody specificity, we performed a competitive phage ELISA to assess which antigen between Δ16HER2 or wtHER2 more successfully competed for the binding of the antibodies. The inhibition curves showed that IgG Δ16ECTM binding to Δ16ECTM phages outweighed their interaction with hECTM phages (Fig. 3H; Supplementary

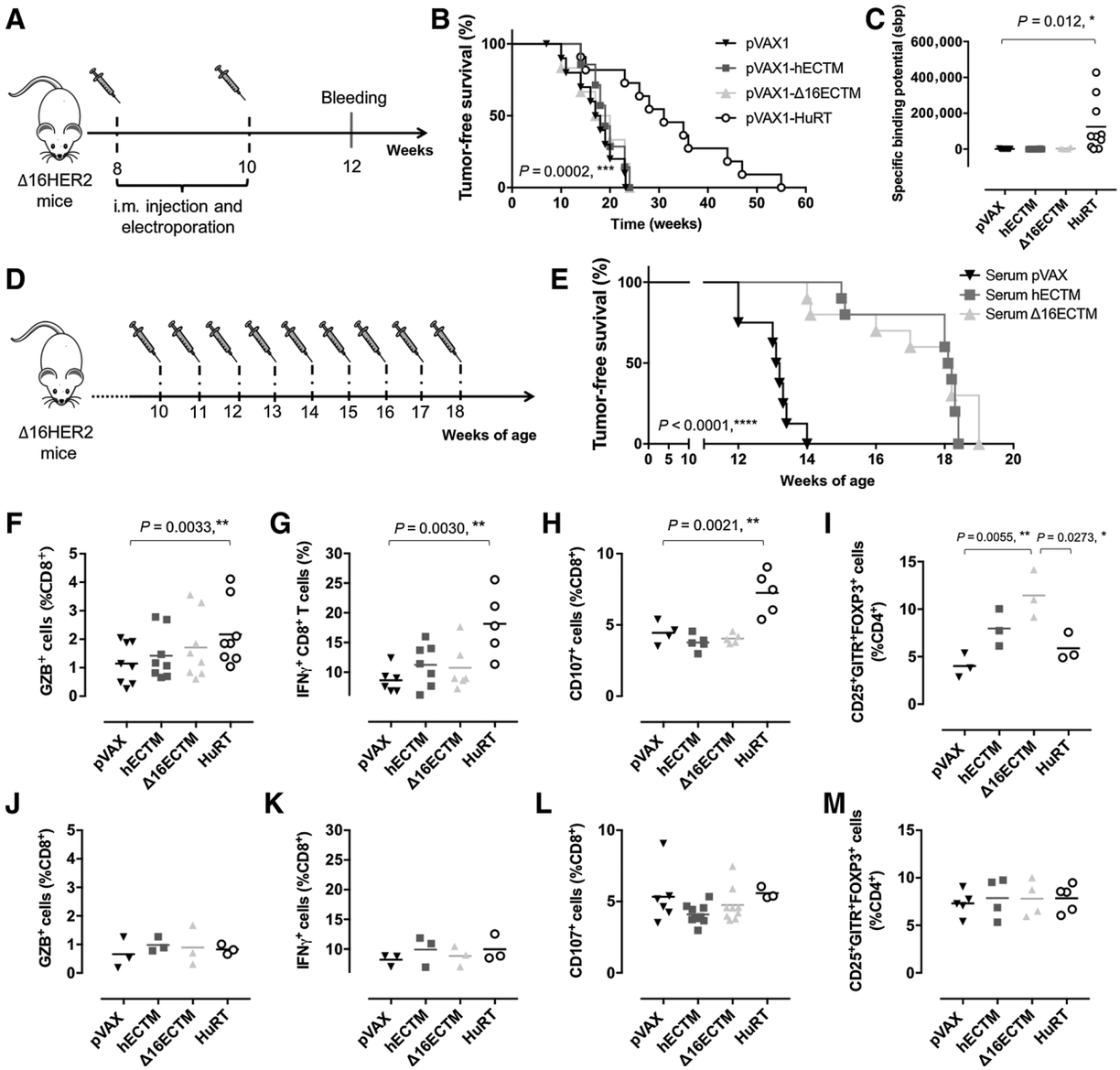

Figure 4.

Immune tolerance impairs DNA vaccination in Δ16HER2 mice. **A,** DNA vaccination schedule on Δ16HER2 mice. Mice (n = 8–14/group) received two i.m. DNA vaccinations at 8 and 10 weeks of age. **B,** Kaplan–Meier curves of Δ16HER2 mice vaccinated with pVAX-HuRT (n = 14), pVAX-hECTM (n = 8), pVAX- Δ16ECTM (n = 8), and pVAX empty vector (n = 8; see Supplementary Table S9 for statistics). **C,** Screening for HER2 antibodies in the sera of immunized mice (pVAX-HuRT *, P = 0.012; see Supplementary Table S10). **D,** Adoptive serum transfer to Δ16HER2 mice (n = 8 mice/group). Ten-week-old Δ16HER2 mice received weekly (for 8 weeks) intraperitoneal injections of immune sera obtained from vaccination of wtFVB mice with pVAX-hECTM, pVAX-Δ16ECTM, and pVAX. **E,** Kaplan–Meier curves of Δ16HER2 mice that received immune pVAX-hECTM, pVAX-Δ16ECTM, and pVAX sera of vaccinated wtFVB mice (log-rank; ****, P < 0.0001; see Supplementary Table S12 for multiple comparisons). **F,** Immunization-induced granzyme B (GZB) expression by T cells. DCs transfected with pVAX, pVAX-hECTM, pVAX-Δ16ECTM, or pVAX-HuRT were incubated with splenocytes isolated from transgenic mice immunized with the corresponding vaccine (n = 8 mice/group; pVAX-HuRT; **, P = 0.0033; Supplementary Table S13). **G,** Immunization-induced IFNγ expression by T cells (pVAX-HuRT **, P = 0.0030; see Supplementary Table S14). **H,** Immunization-induced CD107 exposure on T cells (pVAX-HuRT; **, P = 0.0021; see Supplementary Table S15). **I,** Assessment of the Treg compartment. FACS analysis of the CD4$^+$CD25$^+$FOXP3$^+$ Treg frequency (pVAX-Δ16ECTM and pVAX-hECTM; ****, P < 0.0001; see Supplementary Table S16). **J–M,** Negative control for GZB assay, IFNγ and CD107 using wtFVB splenocytes (P > 0.05; n.s.). Data of each panel are representative of three independent experiments.

Published OnlineFirst October 16, 2018; DOI: 10.1158/2326-6066.CIR-18-0179

Table S8), although these latter phages more effectively competed with Δ16ECTM phages for capturing IgG hECTM (Fig. 3I; Supplementary Table S8). These data demonstrate that it is possible to induce a specific antibody response against Δ16HER2, although it is only 16 residues shorter than wtHER2.

Immune tolerance impairs DNA vaccination in Δ16HER2 transgenic mice

Because pVAX-Δ16ECTM and pVAX-hECTM elicited protective immunity against transplantable Δ16HER2$^+$ tumors, we asked whether they also triggered protection against autochthonous carcinogenesis in Δ16HER2 transgenic mice. These mice, which express the human Δ16HER2 transgene and develop spontaneous mammary carcinomas at 15 weeks of age on average (18), were vaccinated at 8 and 10 weeks of age, when they were still free from mammary lesions (Fig. 4A). pVAX-HuRT was the only vaccine able to delay tumor onset until 25 weeks of age in 50% of animals. However, such protection declined thereafter, and all the mice developed mammary carcinomas at about 9 months of age (Fig. 4B; Supplementary Table S9). pVAX-hECTM and pVAX-Δ16ECTM vaccines failed to elicit a protective immunity leading to 100% tumor penetrance within 25 weeks of age (Fig. 4B). In agreement, HER2 antibodies were detected only in sera collected from pVAX-HuRT immunized mice (Fig. 4C, *, $P = 0.012$; see Supplementary Table S10), and consistent with the chimeric nature of the vaccine, these antibodies were directed against both the human and the rat HER2 protein. In particular, antibodies specific for the human HER2 were the most abundant, with the IgG2a subtype being predominant and the IgG1 class being the dominant subtype (Supplementary Fig. S3A). We also evaluated the ADCC of the sera of DNA-vaccinated mice, using the carboxyfluorescein succinimidyl ester (CFSE)-based method and Cam6 cells as target cells. Consistent with the *in vivo* observations, pVAX-HuRT (blue) was the only vaccine to significantly induce ADCC activity (Supplementary Fig. S3B, **, $P = 0.0025$; see Supplementary Table S11). Δ16HER2 mice, which weekly received immune sera from wtFVB mice vaccinated with pVAX-Δ16ECTM or pVAX-hECTM (Fig. 4D), experienced a significant delay in the tumor onset (****, $P < 0.0001$; Fig. 4E; Supplementary Table S12). In particular, mice treated for 8 weeks with sera derived from pVAX-vaccinated wtFVB mice developed at least one palpable mammary tumor within the 15th week of age, whereas administration of immune sera from wtFVB mice vaccinated with pVAX-Δ16ECTM or pVAX-hECTM resulted in a 4-week delayed tumor onset (Fig. 4E). These results confirm the role of antibodies against HER2-driven carcinogenesis (36) and suggest that tolerogenic mechanisms are operating in Δ16HER2 mice.

We then investigated the functional status of CD8$^+$ T cells upon DNA vaccination. To reproduce antigen presentation *in vitro*, we first transfected dendritic cells (DCs) with pVAX, pVAX-hECTM, pVAX-Δ16ECTM, or pVAX-HuRT, and then we cocultured them with CD8$^+$T cells isolated from Δ16HER2 mice immunized with the corresponding vaccine. Upon activation with DCs, granzyme B (GZB)- and interferon-γ (IFNγ)-positive CD8$^+$ T cells (Fig. 4F and G) showed a significant increase uniquely in the pVAX-HuRT group but not in pVAX-hECTM and pVAX-Δ16ECTM immunized mice (Fig. 4F and Supplementary Table S13; Fig. 4G and Supplementary Table S14, respectively). We also measured the exposure of CD107 on CD8$^+$ T cells as readout of cytotoxic granules degranulation (Fig. 4H and Supplementary Table S15; ref. 37). CD107$^+$CD8$^+$T cell amounts were the same as the negative controls after coculture with DCs transfected with pVAX-hECTM and pVAX-Δ16ECTM, suggesting impaired degranulation. As expected, only DCs transfected with pVAX-HuRT were able to activate CD8$^+$T cells (from pVAX-HuRT vaccinated mice), leading to an increase in the percentage of CD107$^+$CD8$^+$ T cells (**, $P = 0.0021$; Fig. 4H). Then, we verified the contribution of FOXP3$^+$ regulatory T cells (Treg) because they are indispensable for the maintenance of self-tolerance (38). The percentage of CD25$^+$FoxP3$^+$CD4$^+$ Tregs was increased in splenocytes derived from mice immunized with pVAX-hECTM and pVAX Δ16ECTM (Fig. 4I; Supplementary Table S16). Splenocytes from wtFVB mice were taken as control for all the above-mentioned experiments (Fig. 4J–M).

We also investigated Th1/Th2/Th17 CD4$^+$ T cells in immunized mice. We cocultured DCs with lymphocytes from immunized Δ16HER2 mice upon stimulation with anti-CD3 and stained for different markers: IFNγ, IL17, or IL4 (Supplementary Fig. S3C–S3E; Supplementary Table S17). DNA vaccines administered by electroporation induce Th1 response. In accordance, we found a significant increase in T-helper cell type1 (Th1) activity in Δ16HER2-transgenic mice vaccinated with pVAX-HuRT (Supplementary Fig. S3C). This result was expected, considering that Δ16HER2 mice mimic the immunologic tolerance to human HER2 self-antigen. Only the chimeric vaccine pVAX-HuRT broke immune tolerance and induced some immune protection by activating Th1 cells. It is in accordance with the isotype profile associated with pVAX-HuRT immunization, as Th1 polarization has been associated with the production of IgG2a subtype in mice (Supplementary Fig. S3A). The exon deletion itself could not affect MHC sites on Δ16HER2, whether class I, or class II: when aligned by ClustalW, wtHER2, and Δ16HER2 protein sequences shared the same MHC epitopes (Supplementary Fig. S3F).

To investigate central immune tolerance contribution to the failure of pVAX-hECTM and pVAX-Δ16ECTM vaccination in Δ16HER2 mice, we assessed the expression of the human Δ16HER2 transgene in the thymus of 3-week-old mice. Δ16HER2 mRNA was detected in the thymus of transgenic pups, explaining why human Δ16HER2 protein is considered a self-antigen in Δ16HER2 mice (Supplementary Fig. S4A). To consider peripheral tolerogenic mechanisms, we analyzed the expression of CD73, an ectonucleotidase that promotes immunosuppression through adenosine production (39). CD73 was expressed in tumors derived from Δ16HER2 females, and CD73 mRNA positively correlated with tumor size (Supplementary Fig. S4B).

Phages displaying antigen sequences can overcome immune tolerance

To break tolerance and elicit an anticancer immunity, we turned to bacteriophages, which combine high immunogenicity with specificity (40, 41). The phage-treatment regimen comprised of two intraperitoneal injections of 10^{10} PFU/mouse of four different phage preparations—Δ16ECTM, hECTM, Ep6-11 Δ16ECTM, or Ep6-11 hECTM phages—performed at 8 and 10 weeks of age (Fig. 5A). Kaplan–Meier curves showed a significantly prolonged tumor latency period (****, $P < 0.0001$) in all the groups, and in particular, in mice administered with Ep6-11 Δ16ECTM phages (Fig. 5B; Supplementary Table S18, hECTM phages vs. Ep6-11 hECTM phages; *, $P = 0.0359$; Δ16ECTM phages vs. Ep6-11 Δ16ECTM phages; *, $P = 0.0204$). Mice immunized with engineered phages developed

Published OnlineFirst October 16, 2018; DOI: 10.1158/2326-6066.CIR-18-0179

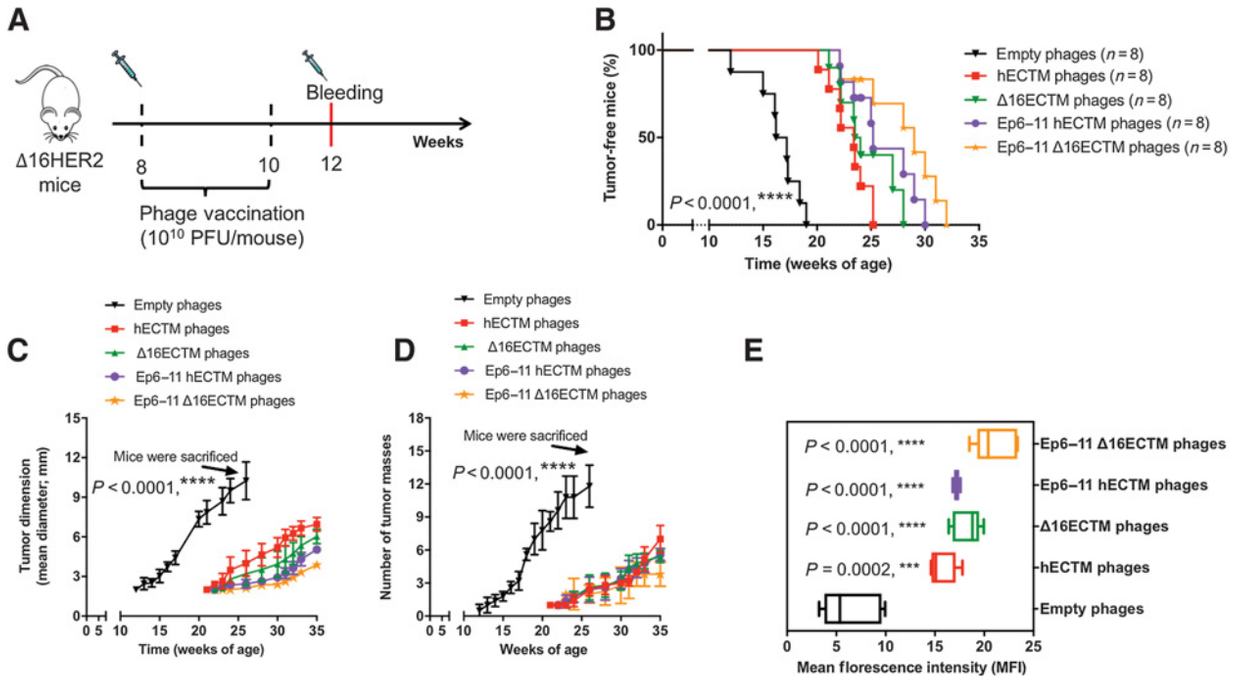

Figure 5.

Phage treatment bypasses immune tolerance and provides protection from Δ16HER2-driven tumorigenesis. **A,** Phage-based vaccination. Δ16HER2 mice ($n = 8$ mice/group) were administered with 10^{10} phages (i.p.) at 8 and 10 weeks of age, prior to tumor onset (8 mice/group). Bleeding occurred at the 12th week of age for antibody screening. **B,** Kaplan–Meier curves of the phage-based vaccines (log-rank; ****, $P < 0.0001$; see Supplementary Table S18). **C,** Tumor growth curves of mice treated with the phage-based vaccines (see Supplementary Table S19). **D,** Tumor multiplicity of mice treated with the phage-based vaccines (see Supplementary Table S20 for statistics). **E,** Antibody detection. Sera of mice (8 mice/group) were pooled together and analyzed by FACS. The *in vivo* outcome correlates with the presence of specific Δ16HER2 antibodies in the sera of treated mice (see Supplementary Table S21).

smaller and fewer tumor masses as compared with the control group (Fig. 5C; Supplementary Table S19; Fig. 5D; Supplementary Table S20; Supplementary Fig. S5A). Because the IgG humoral response to phages has elsewhere been found to peak after the second phage application (42), two weeks after the second administration, sera were collected and screened for the presence of Δ16HER2 antibodies. Although serum antibodies toward Δ16HER2 were detected in all the treated mice (apart from control cohort), mice receiving Ep6-11Δ16ECTM phages showed the most antibodies (Fig. 5E; Supplementary Table S21), in agreement with the conferred antitumor protection.

To analyze the activation status of the other immune compartments in phage-vaccinated mice, we looked at infiltrating CD3$^+$ cells in the tumors (Supplementary Fig. S5B). The count of intratumoral CD3$^+$ cells suggested that phages specific for Δ16HER2 effectively broke the immunotolerance in Δ16HER2 transgenic mice and raised an immune response. Mice given either Δ16ECTM phages or Ep6-11 Δ16ECTM phages had significantly higher numbers of tumor-infiltrating CD3$^+$ cells (Supplementary Fig. S5C; Supplementary Tables S22 and S23). On the contrary, no difference was detected in mice receiving hECTM phages. Among the total infiltrating CD3$^+$ cells, the highest numbers of CD8$^+$T cells were found in the Δ16ECTM phages and Ep6-11 Δ16ECTM phages experimental groups (**, $P = 0.0025$ and ***, $P = 0.0007$, respectively). Mice vaccinated with hECTM and Ep6-11 hECTM phages displayed significantly higher numbers of infiltrating cells than controls (*, $P = 0.034$ and *, $P = 0.0327$, respectively). These data might explain the protection observed *in vivo* with phages targeting wtHER2, especially with Ep6-11 hECTM phages. However, these findings may also imply that CD3$^+$ cells, other than CD8$^+$T cells, might account for the different specificity between hECTM phages and Δ16ECTM phages.

Hence, we evaluated the ADCC response in phage-vaccinated mice as well (Supplementary Fig. S5D). In accordance with data herein reported, only sera from mice which were immunized with Δ16ECTM phages or Ep6-11 Δ16ECTM phages held a significant increase in the ADCC activity (***, $P = 0.0009$ and **, $P = 0.0092$, respectively; Supplementary Table S24). No significant ADCC activity was detected using sera of mice given hECTM phages or Ep6-11 hECTM phages, suggesting that mechanisms other than ADCC account for the *in vivo* protection of these phages. These data further confirm that phages circumvented immunotolerance in Δ16HER2 mice and that Δ16HER2 isoform is immunologically different from wtHER2.

Phage clearance caused a decrease in the viremia of Δ16HER2 transgenic mice 24 hours after phage injection for all the phages under investigation, independently from the exposed antigen sequences (Supplementary Fig. S5E; Supplementary Table S25). These results exclude any interference due to different clearance of phage-based vaccines (Supplementary Fig. S5F). No signs of toxicity (i.e., anaphylactic reactions, changes in core body temperature, etc.) were observed in phage-vaccinated mice. These data demonstrate that phage-displayed vaccines can both overcome immune tolerance and induce a specific antibody response against the Δ16HER2 isoform.

Published OnlineFirst October 16, 2018; DOI: 10.1158/2326-6066.CIR-18-0179

Discussion

Among strategies to undermine cancer morbidity and mortality, DNA vaccines hold considerable potential, combining some of the most desirable features of standard vaccines: they are stable, relatively inexpensive, simple to purify, and able to elicit both cellular and humoral responses (43, 44). The functional and structural characteristics of the TK receptor HER2 make it a good target for cancer DNA vaccination. HER2 is a TM receptor selectively overexpressed in several carcinomas and plays a causal role in oncogenic transformation. HER2 can be readily targeted both by antibodies and cell-mediated immunity, minimizing the risk of autoimmune attack on healthy tissues (45). On the other hand, HER2 is a self-molecule. Therefore, triggering a stable and strong immune response to it must circumvent tolerance mechanisms (33, 46).

DNA vaccines against HER2 succeeded in the prevention of tumor growth in both transplantable tumor models and HER2 transgenic mice (36, 47). DNA vaccination with plasmids, encoding soluble or membrane-bound forms of HER2/neu, led to promising results (36, 48, 49). The present study investigated the feasibility of a DNA vaccine–based strategy against the Δ16HER2 isoform. This goal required insights into the target antigen. Although wtHER2 structure has been characterized (50), the knowledge of Δ16HER2 structure is limited. Using *in silico* techniques, we showed how the deletion of 16 amino acids changes HER2 structure, rendering the ECD of Δ16HER2 more flexible and mobile than the ECD of wtHER2. These structural differences between Δ16HER2 and wtHER2 provide the rationale to design specific therapies targeting Δ16HER2. Thus, we constructed and tested anti-Δ16HER2 DNA vaccines, demonstrating that DNA vaccination is effective against Δ16HER2-expressing Cam6 cells transplanted in syngeneic wtFVB mice. Taking advantage of the LFPD technology, we analyzed the antigen-binding properties of the IgGs induced by vaccination of wtFVB mice with plasmids encoding wtHER2 or Δ16HER2 immunogenic portions. The data prove that IgGs purified from sera of pVAX-Δ16ECTM vaccinated mice bind more often and with greater affinity to Δ16HER2 than the IgGs elicited by pVAX-hECTM, indicating that it is possible to induce a specific anti-Δ16HER2 response. However, these DNA vaccines failed to induce immune protection in Δ16HER2 transgenic mice, suggesting that Δ16HER2 mice recapitulate patients' immunotolerance (32). We found that Δ16HER2 transgenic mice express the transgene early in life in their thymus and develop mammary adenocarcinomas enriched in CD73, which can be considered hallmarks of central (51, 52) and peripheral tolerance (39, 53), respectively. Accordingly, neither pVAX-Δ16ECTM nor pVAX-hECTM was able to elicit antibody production and trigger the ADCC activity. Vaccination with these plasmids failed to activate cytotoxic $CD8^+$ T cells and $CD4^+$ T cells. The chimeric plasmid pVAX-HuRT was the only vaccine able to evoke an immune response in Δ16HER2 mice. It stimulated a humoral response characterized by high production of IgG2a subclass antibodies through activation of Th1 $CD4^+$ repertoire. pVAX-HuRT also triggered a cytotoxic T-cell functional status (i.e., production of GZB and IFNγ, and exposition of CD107). However, due to its structural characteristics, HuRT does not induce a specific, long-lasting immune response against Δ16HER2, and all the mice developed mammary carcinomas by 9 months of age. To overcome the immune tolerance and trigger a stronger anti-cancer protective immunity, we leveraged phage-based vectors to deliver anti-HER2 vaccines, as they combine high immunogenicity, characteristic of viruses, with the great advantage of specificity.

The proposed system derives from the LFPD technology (17), as it is based on filamentous bacteriophage M13 virions engineered to display on their surface the ECTM domains or specific epitopes of HER2 or Δ16HER2. M13 filamentous bacteriophages are reliable immunogen carriers: they are nonpathogenic, nonlytic viruses that infect and replicate only in *Escherichia coli* cells carrying an F' episome, and, at the same time, they are immunogenic in absence of adjuvants (54). Phages are taken up and processed by antigen-presenting cells (55), eliciting both B cell– and T cell–mediated immunity. Previous reports on anti-MAGE vaccination indicate that engineered filamentous bacteriophage virions increase the immunogenicity of delivered tumor-associated antigens (56). The host cell wall–derived lipopolysaccharide (LPS) and the CpG motifs contained in the phage's genome render the phage particles self-adjuvating (57). Accordingly, phage idiotypic vaccination demonstrated to be safe and capable of evoking tumor-specific immune responses in multiple myeloma patients (58, 59). Here, we reported that anti-HER2 phage-based vaccination significantly extended the tumor latency, reduced the growth rate, and decreased tumor multiplicity in Δ16HER2 mice. Vaccination with phages carrying just the two epitopes 6 and 11 (overlapping the splicing region and the adjacent trastuzumab binding site in Δ16ECTM) had a better result than the immunization with phages displaying the whole ECTM molecule. Sera of vaccinated mice carried Δ16HER2 antibodies in amounts that correlated with the anti-cancer protective efficacy of the different phage-based vaccines. Sera of mice immunized with Ep6-11 Δ16ECTM phages showed antibody titers higher than those detected in mice of the Ep6-11 hECTM group. Consistently, we reported that sera of mice vaccinated with Δ16ECTM phages and Ep6-11 Δ16ECTM phages hold a significant ADCC activity. Vaccination with Δ16ECTM and Ep6-11 Δ16ECTM phages also recruited $CD3^+$ cells to the tumor.

The phage-based vaccines that we developed and described here specifically target Δ16HER2. Although the antitumor performances of anti-HER2 phage–based vaccines might be further improved by increasing the number of boosts or combining DNA and phage administration, these data support the use of phage-display systems in the clinical management of $HER2^+$ breast cancer patients, both as anticancer vaccines and for diagnostic analytics to detect Δ16HER2 antibodies in the serum of breast cancer patients.

Disclosure of Potential Conflicts of Interest

No potential conflicts of interest were disclosed.

Authors' Contributions

Conception and design: C. Bartolacci, C. Andreani, C. Marchini, A. Amici
Development of methodology: C. Bartolacci, C. Andreani, C. Curcio, S. Occhipinti, L. Massaccesi, C. Marchini, A. Amici
Acquisition of data (provided animals, acquired and managed patients, provided facilities, etc.): C. Bartolacci, C. Andreani, C. Curcio, R. Galeazzi, M. Iezzi, M. Tilio, V. Gambini
Analysis and interpretation of data (e.g., statistical analysis, biostatistics, computational analysis): C. Bartolacci, C. Andreani, C. Curcio, L. Massaccesi, M. Giovarelli, R. Galeazzi, M. Iezzi, C. Marchini, A. Amici

Published OnlineFirst October 16, 2018; DOI: 10.1158/2326-6066.CIR-18-0179

Writing, review, and/or revision of the manuscript: C. Bartolacci, C. Andreani, S. Occhipinti, L. Massaccesi, M. Giovarelli, R. Galeazzi, J. Wang, C. Marchini, A. Amici
Administrative, technical, or material support (i.e., reporting or organizing data, constructing databases): C. Bartolacci
Study supervision: C. Marchini, A. Amici

Acknowledgments

We would like to thank Dr. Elda Tagliabue (Istituto Nazionale Tumori di Milano, Italy) for kindly providing HEK293 Δ16HER2, HEK293 wtHER2 cells and anti c-erbB-2 MGR2 monoclonal antibody, and Prof. Pierluigi Lollini (University of Bologna, Italy) for kindly providing N202.1A and N202.1E cells. We would like to acknowledge the School of Advanced Studies (University of Camerino, Italy) for supporting with doctoral fellowships (to C. Bartolacci, C. Andreani, M. Tilio, V. Gambini, and J. Wang).

This work was supported by the Italian Association of Cancer Research (AIRC) (IG 11889 to A. Amici and IG 9366 to M. Giovarelli), F.A.R. of the University of Turin (to M. Giovarelli), Fondazione Umberto Veronesi fellowship (to S. Occhipinti), and University of Camerino.

The costs of publication of this article were defrayed in part by the payment of page charges. This article must therefore be hereby marked *advertisement* in accordance with 18 U.S.C. Section 1734 solely to indicate this fact.

Received March 19, 2018; revised August 8, 2018; accepted October 9, 2018; published first October 16, 2018.

References

1. Sorlie T, Tibshirani R, Parker J, Hastie T, Marron JS, Nobel A, et al. Repeated observation of breast tumor subtypes in independent gene expression data sets. Proc Natl Acad Sci USA 2003;100:8418–23.
2. Yamauchi H, Stearns V, Hayes DF. The role of c-erbB-2 as a predictive factor in breast cancer. Breast Cancer 2001;8:171–83.
3. Siegel R, DeSantis C, Virgo K, Stein K, Mariotto A, Smith T, et al. Cancer treatment and survivorship statistics, 2012. CA Cancer J Clin 2012; 62:220–41.
4. Mendes D, Alves C, Afonso N, Cardoso F, Passos-Coelho JL, Costa L, et al. The benefit of HER2-targeted therapies on overall survival of patients with metastatic HER2-positive breast cancer–a systematic review. Breast Cancer Res 2015;17:140.
5. Rexer BN, Arteaga CL. Intrinsic and acquired resistance to HER2-targeted therapies in HER2 gene-amplified breast cancer: mechanisms and clinical implications. Crit Rev Oncog 2012;17:1–16.
6. Finn OJ. The dawn of vaccines for cancer prevention. Nat Rev Immunol 2018;18:183–94.
7. Mittendorf EA, Peoples GE. Injecting hope–a review of breast cancer vaccines. Oncology 2016;30:475–81, 85.
8. Moasser MM. The oncogene HER2: its signaling and transforming functions and its role in human cancer pathogenesis. Oncogene 2007; 26:6469–87.
9. Castiglioni F, Tagliabue E, Campiglio M, Pupa SM, Balsari A, Menard S. Role of exon-16-deleted HER2 in breast carcinomas. Endocr Relat Cancer 2006;13:221–32.
10. Mitra D, Brumlik MJ, Okamgba SU, Zhu Y, Duplessis TT, Parvani JG, et al. An oncogenic isoform of HER2 associated with locally disseminated breast cancer and trastuzumab resistance. Mol Cancer Ther 2009;8:2152–62.
11. Alajati A, Sausgruber N, Aceto N, Duss S, Sarret S, Voshol H, et al. Mammary tumor formation and metastasis evoked by a HER2 splice variant. Cancer Res 2013;73:5320–7.
12. Ursini-Siegel J, Schade B, Cardiff RD, Muller WJ. Insights from transgenic mouse models of ERBB2-induced breast cancer. Nat Rev Cancer 2007;7:389–97.
13. Siegel PM, Ryan ED, Cardiff RD, Muller WJ. Elevated expression of activated forms of Neu/ErbB-2 and ErbB-3 are involved in the induction of mammary tumors in transgenic mice: implications for human breast cancer. EMBO J 1999;18:2149–64.
14. Kwong KY, Hung MC. A novel splice variant of HER2 with increased transformation activity. Mol Carcinog 1998;23:62–8.
15. Huynh FC, Jones FE. MicroRNA-7 inhibits multiple oncogenic pathways to suppress HER2Delta16 mediated breast tumorigenesis and reverse trastuzumab resistance. PLoS One 2014;9:e114419.
16. Tilio M, Gambini V, Wang J, Garulli C, Kalogris C, Andreani C, et al. Irreversible inhibition of Delta16HER2 is necessary to suppress Delta16-HER2-positive breast carcinomas resistant to lapatinib. Cancer Lett 2016;381:76–84.
17. Gabrielli F, Salvi R, Garulli C, Kalogris C, Arima S, Tardella L, et al. Identification of relevant conformational epitopes on the HER2 oncoprotein by using Large Fragment Phage Display (LFPD). PLoS One 2013;8: e58358.
18. Marchini C, Gabrielli F, Iezzi M, Zenobi S, Montani M, Pietrella L, et al. The human splice variant Delta16HER2 induces rapid tumor onset in a reporter transgenic mouse. PLoS One 2011;6:e18727.
19. Andreani C, Bartolacci C, Wijnant K, Crinelli R, Bianchi M, Magnani M, et al. Resveratrol fuels HER2 and ERalpha-positive breast cancer behaving as proteasome inhibitor. Aging 2017;9:508–23.
20. Bostrom J, Yu SF, Kan D, Appleton BA, Lee CV, Billeci K, et al. Variants of the antibody herceptin that interact with HER2 and VEGF at the antigen binding site. Science 2009;323:1610–4.
21. Fisher RD, Ultsch M, Lingel A, Schaefer G, Shao L, Birtalan S, et al. Structure of the complex between HER2 and an antibody paratope formed by side chains from tryptophan and serine. J Mol Biol 2010;402:217–29.
22. Bocharov EV, Mineev KS, Volynsky PE, Ermolyuk YS, Tkach EN, Sobol AG, et al. Spatial structure of the dimeric transmembrane domain of the growth factor receptor ErbB2 presumably corresponding to the receptor active state. J Biol Chem 2008;283:6950–6.
23. Red Brewer M, Choi SH, Alvarado D, Moravcevic K, Pozzi A, Lemmon MA, et al. The juxtamembrane region of the EGF receptor functions as an activation domain. Mol Cell 2009;34:641–51.
24. Aertgeerts K, Skene R, Yano J, Sang BC, Zou H, Snell G, et al. Structural analysis of the mechanism of inhibition and allosteric activation of the kinase domain of HER2 protein. J Biol Chem 2011;286:18756–65.
25. Uchida Y, Hara M, Nishio H, Sidransky E, Inoue S, Otsuka F, et al. Epidermal sphingomyelins are precursors for selected stratum corneum ceramides. J Lipid Res 2000;41:2071–82.
26. Galeazzi R, Massaccesi L, Piva F, Principato G, Laudadio E. Insights into the influence of 5-HT2c aminoacidic variants with the inhibitory action of serotonin inverse agonists and antagonists. J Mol Model 2014; 20:2120.
27. Fiser A, Sali A. ModLoop: automated modeling of loops in protein structures. Bioinformatics 2003;19:2500–1.
28. Ko J, Park H, Heo L, Seok C. GalaxyWEB server for protein structure prediction and refinement. Nucleic Acids Res 2012;40: W294–7.
29. Biasini M, Bienert S, Waterhouse A, Arnold K, Studer G, Schmidt T, et al. SWISS-MODEL: modelling protein tertiary and quaternary structure using evolutionary information. Nucleic Acids Res 2014;W252–8.
30. Ceroni A, Passerini A, Vullo A, Frasconi P. DISULFIND: a disulfide bonding state and cysteine connectivity prediction server. Nucleic Acids Res 2006;34:W177–81.
31. Jo S, Kim T, Iyer VG, Im W. CHARMM-GUI: a web-based graphical user interface for CHARMM. J Comput Chem 2008;29:1859–65.
32. Disis ML, Shiota FM, Cheever MA. Human HER-2/neu protein immunization circumvents tolerance to rat neu: a vaccine strategy for 'self' tumour antigens. Immunology 1998;93:192–9.
33. Quaglino E, Mastini C, Amici A, Marchini C, Iezzi M, Lanzardo S, et al. A better immune reaction to Erbb-2 tumors is elicited in mice by DNA vaccines encoding rat/human chimeric proteins. Cancer Res 2010;70: 2604–12.
34. Reverberi R, Reverberi L. Factors affecting the antigen-antibody reaction. Blood Transfus 2007;5:227–40.
35. Watson JD. Molecular biology of the gene. San Francisco: Pearson/ Benjamin Cummings; 2003.

Published OnlineFirst October 16, 2018; DOI: 10.1158/2326-6066.CIR-18-0179

36. Rolla S, Marchini C, Malinarich S, Quaglino E, Lanzardo S, Montani M, et al. Protective immunity against neu-positive carcinomas elicited by electroporation of plasmids encoding decreasing fragments of rat neu extracellular domain. Hum Gene Ther 2008;19:229–40.
37. Betts MR, Brenchley JM, Price DA, De Rosa SC, Douek DC, Roederer M, et al. Sensitive and viable identification of antigen-specific CD8+ T cells by a flow cytometric assay for degranulation. J Immunol Methods 2003;281: 65–78.
38. Hori S, Nomura T, Sakaguchi S. Control of regulatory T cell development by the transcription factor Foxp3. Science 2003;299:1057–61.
39. Allard D, Allard B, Gaudreau PO, Chrobak P, Stagg J. CD73-adenosine: a next-generation target in immuno-oncology. Immunotherapy 2016;8: 145–63.
40. Wu Y, Wan Y, Bian J, Zhao J, Jia Z, Zhou L, et al. Phage display particles expressing tumor-specific antigens induce preventive and therapeutic anti-tumor immunity in murine p815 model. Int J Cancer 2002;98: 748–53.
41. Fang J, Wang G, Yang Q, Song J, Wang Y, Wang L. The potential of phage display virions expressing malignant tumor specific antigen MAGE-A1 epitope in murine model. Vaccine 2005;23:4860–6.
42. Hodyra-Stefaniak K, Miernikiewicz P, Drapala J, Drab M, Jonczyk-Matysiak E, Lecion D, et al. Mammalian Host-Versus-Phage immune response determines phage fate in vivo. Sci Rep 2015;5:14802.
43. Liu MA, Ulmer JB. Human clinical trials of plasmid DNA vaccines. Adv Genet 2005;55:25–40.
44. Marchini C, Kalogris C, Garulli C, Pietrella L, Gabrielli F, Curcio C, et al. Tailoring DNA vaccines: designing strategies against HER2-positive cancers. Front Oncol 2013;3:122.
45. Lollini PL, Forni G. Cancer immunoprevention: tracking down persistent tumor antigens. Trends Immunol 2003;24:62–6.
46. Occhipinti S, Sponton L, Rolla S, Caorsi C, Novarino A, Donadio M, et al. Chimeric rat/human HER2 efficiently circumvents HER2 tolerance in cancer patients. Clin Cancer Res 2014;20:2910–21.
47. Quaglino E, Mastini C, Forni G, Cavallo F. ErbB2 transgenic mice: a tool for investigation of the immune prevention and treatment of mammary carcinomas. Curr Protoc Immunol 2008;Chapter 20:Unit 20.9.1-20.9-10.
48. Chen Y, Hu D, Eling DJ, Robbins J, Kipps TJ. DNA vaccines encoding full-length or truncated Neu induce protective immunity against Neu-expressing mammary tumors. Cancer Res 1998;58:1965–71.
49. Quaglino E, Iezzi M, Mastini C, Amici A, Pericle F, Di Carlo E, et al. Electroporated DNA vaccine clears away multifocal mammary carcinomas in her-2/neu transgenic mice. Cancer Res 2004;64:2858–64.
50. Cho HS, Mason K, Ramyar KX, Stanley AM, Gabelli SB, Denney DW Jr, et al. Structure of the extracellular region of HER2 alone and in complex with the Herceptin Fab. Nature 2003;421:756–60.
51. Reilly RT, Gottlieb MB, Ercolini AM, Machiels JP, Kane CE, Okoye FI, et al. HER-2/neu is a tumor rejection target in tolerized HER-2/neu transgenic mice. Cancer Res 2000;60:3569–76.
52. Anderson MS, Venanzi ES, Klein L, Chen Z, Berzins SP, Turley SJ, et al. Projection of an immunological self shadow within the thymus by the aire protein. Science 2002;298:1395–401.
53. Jin D, Fan J, Wang L, Thompson LF, Liu A, Daniel BJ, et al. CD73 on tumor cells impairs antitumor T-cell responses: a novel mechanism of tumor-induced immune suppression. Cancer Res 2010;70:2245–55.
54. Meynell GG, Lawn AM. Filamentous Phages specific for the I Sex Factor. Nature 1968;217:1184–6.
55. Gao J, Wang Y, Liu Z, Wang Z. Phage display and its application in vaccine design. Ann Microbiol 2010;60:13–9.
56. Sartorius R, Pisu P, D'Apice L, Pizzella L, Romano C, Cortese G, et al. The use of filamentous bacteriophage fd to deliver MAGE-A10 or MAGE-A3 HLA-A2-restricted peptides and to induce strong antitumor CTL responses. J Immunol 2008;180:3719–28.
57. Grabowska AM, Jennings R, Laing P, Darsley M, Jameson CL, Swift L, et al. Immunisation with phage displaying peptides representing single epitopes of the glycoprotein G can give rise to partial protective immunity to HSV-2. Virology 2000;269:47–53.
58. Roehnisch T, Then C, Nagel W, Blumenthal C, Braciak T, Donzeau M, et al. Phage idiotype vaccination: first phase I/II clinical trial in patients with multiple myeloma. J Transl Med 2014;12:119.
59. Jacob JB, Quaglino E, Radkevich-Brown O, Jones RF, Piechocki MP, Reyes JD, et al. Combining human and rat sequences in her-2 DNA vaccines blunts immune tolerance and drives antitumor immunity. Cancer Res 2010;70:119–28.

Published OnlineFirst October 16, 2018; DOI: 10.1158/2326-6066.CIR-18-0179

Cancer Immunology Research

Phage-Based Anti-HER2 Vaccination Can Circumvent Immune Tolerance against Breast Cancer

Caterina Bartolacci, Cristina Andreani, Claudia Curcio, et al.

Cancer Immunol Res 2018;6:1486-1498. Published OnlineFirst October 16, 2018.